Carbon monoxide oxidation on Rh(111): Velocity and angular distributions of the CO_2 product

J. I. Colonell, K. D. Gibson, and S. J. Sibener
The James Franck Institute and the Department of Chemistry, The University of Chicago, Chicago, Illinois 60637

(Received 5 June 1995; accepted 18 July 1995)

The velocity and angular distributions of CO_2 produced by CO oxidation on Rh(111) have been measured as a function of surface temperature and oxygen coverage. Both the velocity and angular distributions are bimodal. The velocities of one component are well fit by a Maxwell–Boltzmann distribution at the surface temperature, and the angular distribution of its intensity is cosine. The second component is non-Boltzmann, and the angular distribution is sharply peaked toward normal. The average energy of this feature is a very strong function of the surface temperature, increasing with a slope of $8.7k_b$, where k_b is the Boltzmann constant, between 475 K and 700 K. Surprisal analysis proves useful in condensing and interpreting these data. © *1995 American Institute of Physics.*

I. INTRODUCTION

The energy disposal into the final gas phase products of a surface reaction is largely determined by the part of the potential energy surface which governs the last step of the reaction. If the product is trapped on the surface after it is formed and the final step is the desorption of the physisorbed molecule, the velocity and internal state distributions will be close to Maxwell–Boltzmann distributions at the surface temperature and the angular distribution will be cosine. If the products desorb without first accommodating on the surface, the velocity, angular, and internal state distributions may yield information about the potential energy surface closer to the transition state between adsorbed reactants and products.

The dynamics of CO oxidation on transition metal surfaces is of interest both from a fundamental and a practical point of view. CO_2 formation serves as a model recombination reaction with a large barrier and substantial exothermicity, and transition metals are used to catalyze this reaction in practical applications, e.g., automotive catalytic converters. It is also one of the most thoroughly studied surface reactions. The kinetics of CO oxidation have been studied on many different surfaces under a wide variety of conditions.[1,2] The dynamics of the reaction have also been examined, primarily on Pt, Rh, and Pd surfaces.

CO oxidation is known to produce angular distributions more sharply peaked than cosine on Pt(111) (Refs. 3–5) and Rh(111);[6,7] on Pd(111) the CO_2 desorbs in a nearly cosine distribution.[8] Velocity distributions have been measured for both Pt (Refs. 9–12) and Rh (Ref. 7) surfaces at high temperatures, and on Pt(111),[13] Pd(110),[14] and Pt(110) (1×2) (Refs. 14, 15) during temperature programmed reactions. All show translational energies greater than expected for molecules which have accommodated at the surface temperature. The vibrational and rotational energy distributions of product CO_2 have been measured for polycrystalline Pt,[16–22] Rh,[21] and Pd.[18,21,22] On all three surfaces, vibrational and rotational temperatures are greater than the surface temperature.

For the particular case of CO oxidation on Rh(111), at surface temperatures in the range 700–1000 K, Brown and Sibener[7] measured kinetic energies of CO_2 desorbing at normal of about 8.5 kcal/mol (370 meV). The translational energy was found to decrease rapidly with increasing desorption angle. Coulston and Haller[21] measured the IR chemiluminescence spectra of CO_2 produced by CO oxidation on Pd, Pt, and Rh foils. On Rh at 584 K, they report vibrational temperatures of about 1250 K for the antisymmetric and symmetric stretching modes and the bending modes. The rotational temperature measured was 730 K, also substantially greater than the surface temperature. These studies of CO oxidation on Rh indicate that there is a barrier to the reaction, and that much of the energy is released with the CO_2 molecule instead of into surface modes. The high vibrational temperatures suggest that the carbon oxygen bonds in the transition state are longer than in the CO_2 molecule, and that the transition state is bent.

The impetus for the current work was to measure the CO_2 velocity distributions under steady state conditions, known oxygen coverages, and over a broad temperature range. Most earlier studies[7,9–12] measured the CO_2 time-of-flight (TOF) by chopping the incoming CO beam, so it was not possible to separate the residence time of the CO from the time of flight of the product CO_2. The residence time of the CO is substantial ($>2\ \mu$s) below 800 K, so this method is limited to very high temperatures. In addition, chopping the incoming beam causes the oxygen and CO coverages to change during the measurement. More recently, TOF spectra measured by chopping the product flux during temperature programmed reactions have been reported.[13–15] This technique is able to access very high coverages of the reactants, but the measurements must be made under conditions of changing reactant coverages and surface temperature. Also, it is difficult to access the same reactant coverages at different surface temperatures. In this work, we measure the CO_2 time-of-flight distributions by chopping the product flux after the crystal; thus the measurement is decoupled from the CO residence time, allowing measurements even at low surface temperatures. We use continuous beams of O_2 and CO, and therefore have constant coverages of the reactants on the surface. We are also able to measure the oxygen coverage

and verify that our measurements at different temperatures are performed with the same surface oxygen coverage. Thus we are able to measure the product velocity distributions as a function of oxygen coverage and surface temperature.

II. EXPERIMENT

These experiments were performed in a molecular beam scattering machine which has been described previously.[23,24] Only the modifications made for these experiments will be described in detail here. The UHV scattering chamber is pumped by a 400 l /s ion pump and a TSP and contains the three axis crystal manipulator and independently rotatable differentially pumped quadrupole mass spectrometer detector. Continuous beams of CO and oxygen are produced by supersonic expansion in the source chamber. The beams are in a plane perpendicular to the scattering plane, one in the scattering plane (the center beam) which can be chopped before the crystal, and the other inclined by 15°. The beam spots overlap at the crystal and are about 5 mm in diameter. The intensity of the beams, estimated from measurements of Ar beams in ion gauge fluxmeters, is about 10^{13}–10^{14}/s, or about 0.1–1 ML/s. The crystal may be moved out of the path of the center beam and the detector rotated to measure the velocity distribution of the incident beam directly.

A doubly-differentially pumped postcrystal chopper was added for these experiments. An ion pumped housing containing the motor (an ac hysteresis motor with high temperature windings) a small light bulb and photodiode is bolted to the detector and rotates with it. A small slotted disk on one end of the motor shaft interrupts the light from the bulb which is detected by the photodiode to create the trigger signal. The other end of the motor shaft extends through a second ion pumped region into the scattering chamber, where the cross-correlation chopper is keyed to it. The chopper interrupts the product flux from the crystal 10.5 cm from the ionizer of the mass spectrometer. A schematic of the experimental setup is shown in Fig. 1.

The ion flight time was determined by measuring the TOF spectra of fully expanded beams of He, Ne, and Ar using the source chopper, for which the chopper–ionizer distance was known. The distance from the postcrystal chopper to the ionizer and the time delay between the trigger pulse and the start of the cross-correlation pattern was determined by measuring time of flight spectra of the same molecular beam with both the postcrystal chopper and the source chopper. Both the slotted disk which creates the trigger signal and the cross correlation chopper are keyed to the motor shaft, so that their relative position is fixed. However, the trigger delay is a function of the chopper frequency and the current supplied to the light bulb, so this delay was measured each day by comparing TOF spectra of a direct beam measured with the source chopper and with the postcrystal chopper.

The TOF spectra were measured using standard cross-correlation time-of-flight techniques. The wheel pattern is a pseudorandom sequence of 511 slots and holes derived in our group.[25] The chopper motor was controlled by a sine wave from a digital signal generator which was amplified by an audio amplifier. A 20 MHz clock provided the time base for both the signal generator and the custom CAMAC electronics which controlled two Ortec ACE-MCS boards counting alternate chopper cycles; two MCS boards were used to eliminate counting dead time between cycles. The chopper frequency used in all of these experiments was 195.69 Hz, producing a channel time of 10 μs.

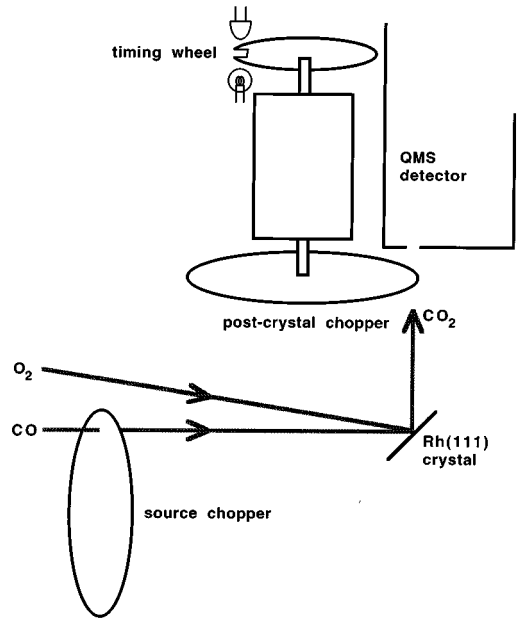

FIG. 1. Schematic of experimental setup. Time-of-flight spectra may be measured either by chopping the beam with the source chopper before the crystal, or by chopping the product flux after the crystal with the postcrystal cross-correlation chopper.

The measured TOF spectrum is a convolution of the gate function of the chopper (the chopper pattern convolved with the detector aperture) and the ionizer broadening (the molecules may be ionized anywhere along the finite length of the ionizer). The gate function was measured directly by detecting light passing through the chopper and detector aperture with a photomultiplier. The ionizer broadening is modeled by convolving the velocity distribution with a square. The electron impact ionizer detects the density of molecules, so the signal must be weighted by the ionization probability, which is inversely proportional to the velocity. The TOF spectra are fit by first subtracting out the ion flight time and the trigger delay, deconvolving the measured spectrum from the gate function (by convolving with the inverse of the measured gate function), and fitting the result to

$$f(t)=\left(\frac{1}{t^2}\right)\left(\frac{t}{\text{chopper–ionizer distance}}\right)\times[f(v)]^{*}(\text{ionizer broadening}). \tag{1}$$

The factor of $(1/t^2)$ is the Jacobian for changing variables from velocity to time. The fitting program used is a least-squares routine based on MRQMIN from Numerical Recipes.[26] The functional forms chosen for $f(v)$ will be discussed in detail later. All of the intensities in this paper come from integration of velocity distributions from these fits, and so are flux corrected.

The angular acceptance of the detector is about 1 deg. With the beams incident on the crystal at 45° and the detector at normal, the beam spot completely fills the detector aperture. The size of the spot seen by the detector varies as $[1/\cos(\theta_f)]$, where θ_f is the angle measured with respect to the surface normal. At large angles, the beam spot is no longer larger than the detector spot. The intensities as a function of angle were corrected by calculating the fraction of the detector view filled by the beam from the known geometry of the apparatus, and this correction was checked by measuring the angular distribution of water desorbing from water multilayers, which is assumed to be cosine distributed.

The Rh(111) sample (Cornell Materials Preparation Lab) was cut and polished to within 1° of the (111) face and checked by x-ray Laue back reflection. The primary contaminants were S, B, and C. S and B were removed by cycles of Ar^+ sputtering (10 μA, 900 K) followed by annealing at 1300 K. C was removed daily by exposing the crystal to oxygen at 900 K and annealing at 1300 K. Oxygen absorbed into the bulk of the sample was removed by annealing the crystal at 1300 K for 3 min between measurements. Cleanliness was checked by Auger, and surface flatness by He reflectivity.

In these experiments, the reactants were supplied to the surface using continuous beams of carbon monoxide and oxygen with an incident angle of 45°. The steady state coverage of oxygen was controlled by adjusting the intensity of the two beams at a given temperature. The oxygen coverage was measured by titration—after establishing a steady-state coverage with both beams on, the O_2 beam was flagged off while monitoring the CO_2 signal. The integrated signal was compared with that from titrating off a saturated (0.5 ML) oxygen overlayer.[27] The CO coverage is unknown; some must be adsorbed since CO oxidation occurs via a Langmuir–Hinshelwood mechanism on this surface,[6] but it desorbs readily at these temperatures.[28,29] Oxygen dissociates completely at these temperatures, and may form an ordered overlayer at θ_O=oxygen coverage $\sim$0.25 ML below 500 K,[30–32] but it is not known if there is any ordering in mixed CO–O overlayers.

Counting times for spectra at desorption angles near zero degrees were 15 min ($\sim 2\times10^5$ shots). The TOF spectra at larger desorption angles required longer counting times (30 min–1 h). The crystal was always annealed after every 15 min of data collection to remove absorbed oxygen from the bulk.

III. RESULTS

Time-of-flight distributions of the CO_2 product were measured as a function of desorption angle for surface temperatures from 475 K to 1000 K and oxygen coverages from 0.1 to 0.33 ML. For Rh(111) in this temperature range, the saturation coverage of oxygen is 0.5 ML. Some typical data for 475 K and $\theta_O \sim 0.1$ ML are shown in Fig. 2. At angles far from normal ($\theta_f > 60$) the distributions are well fit by Maxwell–Boltzmann distributions at the surface temperature,

$$f(v) = N v^3 \exp\left(\frac{-mv^2}{2k_bT_s}\right), \tag{2}$$

where m is the mass of the desorbing molecule, T_s is the surface temperature, k_b is the Boltzmann constant, and N is a normalization factor. At angles nearer normal, the TOFs could be fit only by a product of a shifted Boltzmann and low order Hermite polynomials,

$$f(v) = N\left[1 + \sum_{i=3}^{9} n_i H_i(v)\right] v^3 \exp\left[-\left(\frac{v-v_0}{\alpha}\right)^2\right]. \tag{3}$$

Fitting the TOF spectra to this form offers no physical insight, but it does adequately model the data and provides a convenient way to integrate the spectra to calculate total intensity, average energy, and speed ratio. The speed ratio, frequently used to characterize the width of a velocity distribution, is the ratio of the standard deviation of the measured distribution and the standard deviation of a Maxwell–Boltzmann distribution with the same average energy,

$$\mathrm{SR} = \sqrt{\frac{\left(\frac{2\langle E\rangle}{m\langle v\rangle^2}\right) - 1}{\left(\frac{32}{9\pi}\right) - 1}}. \tag{4}$$

The average energy and speed ratio are plotted as a function of desorption angle in Fig. 3. The average energy drops sharply as a function of angle, approaching the Maxwellian value of $2k_bT_s$ at large angles. The speed ratio, curiously, is greater than 1 at most angles, and peaks near $\theta_f = 30°$. The angular distribution is shown in Fig. 4, and is best fit by the bimodal form,

$$f(\theta_f) = a\,\cos^n(\theta_f) + (1-a)\cos(\theta_f) \tag{5}$$

with $n \sim 9$ and $a \sim 0.7$. Brown and Sibener[6] measured $n \sim 12$ and $a \sim 0.65$ at $T_s = 550$ K; the difference is probably due to a difference in oxygen coverage. Results are similar at other temperatures. n is independent of temperature, while a increases with increasing surface temperature.

The bimodal form of the angular distribution and the odd behavior of the speed ratio suggest that the TOF distributions are actually the sum of two distributions; one a Maxwell–Boltzmann at T_s which has a cosine angular distribution and dominates at large θ_f, and the other a higher energy component which is sharply peaked at normal, with a $\cos^9(\theta_f)$ angular distribution. The functional form of the velocity distribution suggested by this hypothesis is

$$f(v) = N_1 v^3 \exp\left[-\left(\frac{v-v_0}{\alpha}\right)^2\right] + N_2(\theta_f = 75)\,\frac{\cos(\theta_f)}{\cos(75)}\,v^3 \exp\left(\frac{-mv^2}{2k_bT_s}\right), \tag{6}$$

where $N_2(\theta_f = 75)$ is the scaling factor of the velocity distribution at a desorption angle of 75°. We have scaled the intensity of the thermal distribution assuming that its angular distribution is cosine. The velocity distribution of the high energy portion is well fit by a simple shifted Boltzmann, and the fit is not improved by the addition of Hermite polynomi-

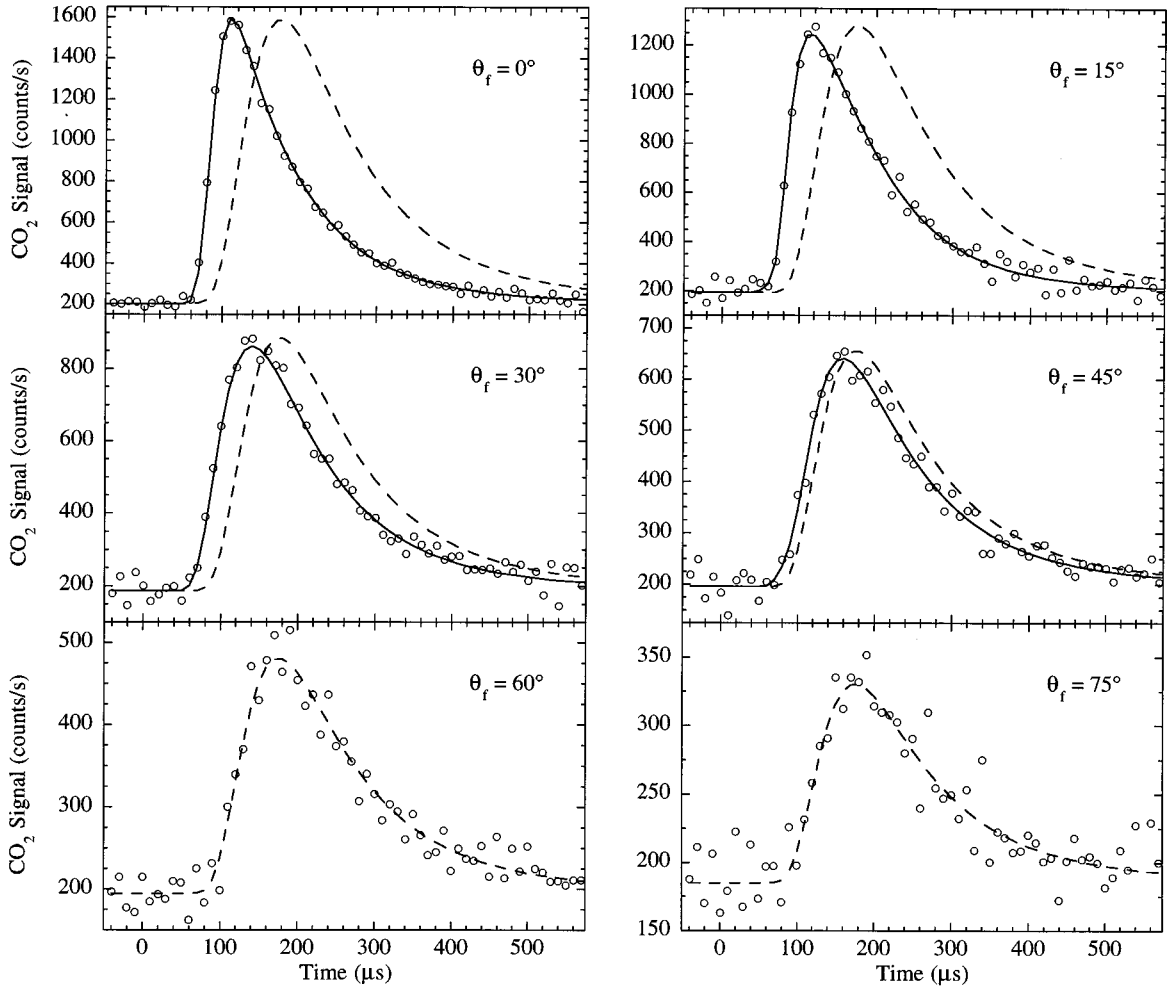

FIG. 2. TOF spectra at T_s=475 K, θ_O~0.1 ML and different desorption angles, deconvolved from the gate function. The solid lines are fit to the form in Eq. (3). The dashed curves depict Maxwell–Boltzmann distributions at the surface temperature.

als. N_1, α, and v_0 are still functions of θ_f. TOF distributions at T_s=500 K and θ_O~0.1 ML are shown along with fits to Eq. (6) in Fig. 5.

The fraction of the thermally distributed product can be calculated by integrating over the two angular distributions. The results, as a function of T_s and oxygen coverage, are shown in Fig. 6. At θ_O~0.1 ML, the thermal fraction clearly decreases with increasing T_s. The results at higher coverages are also shown, but the signal levels are too small to determine the relative intensities accurately, and no clear trend can be seen.

We concentrate now on the behavior of the high energy part of the velocity distributions. Its average energy as a function of desorption angle is shown in Fig. 7; it decreases slowly with increasing desorption angle. The speed ratio increases with desorption angle. The average energy at normal for the high energy peak is shown as a function of oxygen coverage in Fig. 8; the energy increases slowly with increasing oxygen coverage. The speed ratio decreases at higher oxygen coverages.

The most striking result, however, is the temperature dependence of the energy of the high energy peak, which is plotted for θ_O~0.1 ML and θ_f=0° in Fig. 9. Remarkably, for T_s<700 K, the average energy increases at a rate of $8.7k_b$, four-times the increase expected for molecules which are accommodating at the surface temperature. Even if we take the average energy over the whole velocity distribution, instead of just the high energy component, the average energy increases at a rate of $\sim 9k_b$. The unexpectedly strong dependence of the energy on the surface temperature is not dependent on the bimodal analysis of the data.

Above 700 K, the slope decreases. At higher T_s we only have average energies of the whole TOF spectrum because the intensities are too small to get a reliable measurement of the intensity of the thermally distributed CO_2. The fraction of thermally distributed product decreases with increasing temperature, so the error introduced in the average energy is probably <10%. The slope of $\langle E \rangle$ vs T_s is substantial even for T_s>700 K, which disagrees with earlier results for this system[7] which reported no temperature dependence of the velocity distributions. These earlier measurements were made at constant beam intensity instead of at constant coverage. Approximating those conditions, we could reproduce their measurements, and found that the oxygen coverage is a

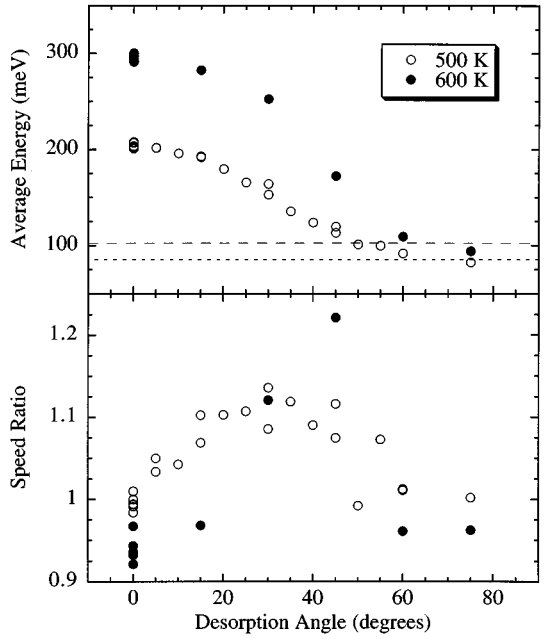

FIG. 3. The top panel shows the variation of the average energy as a function of desorption angle; the short and long dashed lines indicate $2k_bT_s$ at 500 K and 600 K, respectively. The lower panel shows the speed ratio. Open circles, $\theta_O \sim 0.1$ ML, $T_s = 500$ K; filled circles, $\theta_O \sim 0.1$ ML, $T_s = 600$ K.

function of temperature (the oxygen coverage is smaller at higher temperatures because oxygen absorbs into the bulk more quickly). The difference in oxygen coverage accounts for the difference between the current results and Ref. 7.

The behavior of the average energy is similar at higher oxygen coverages, as seen in Fig. 10, and the slope even increases for $\theta_f \sim 0.3$ ML. We also looked at the CO+NO reaction at oxygen coverages of ~0.1, and found velocity distributions identical to those for CO+O. We looked for effects of oxygen absorbed into the bulk of the Rh crystal by loading the bulk with oxygen by dosing with an oxygen beam for 15 min before the measurement and obtained results very similar to those for the clean surface.

In order to learn something about physisorbed CO_2, we also measured TOF spectra for He seeded CO_2 scattering from the clean Rh(111) surface at the same surface temperatures as our CO oxidation measurements. The results are presented in Fig. 11; the incident angle is 45°, and the average energy of the incident CO_2 beam is 430 meV. At $\theta_f = 0°$, there is a clear trapping-desorption component along with a peak due to directly scattered CO_2. The trapping component is well fit by a Maxwell–Boltzmann velocity distribution at the surface temperature, and its relative intensity decreases with increasing T_s.

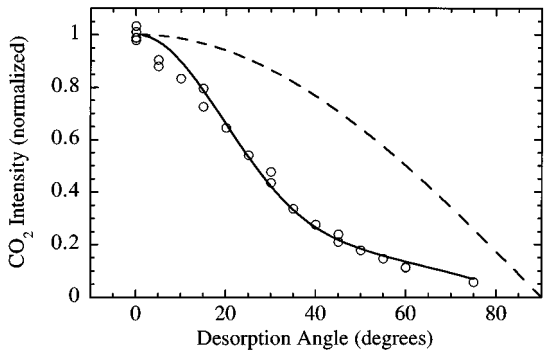

FIG. 4. Angular distribution of CO_2 intensity for $\theta_O \sim 0.1$ ML, $T_s = 500$ K. The solid line is a fit to Eq. (5) with $n = 9.4$, $a = 0.73$. The dashed line shows $\cos(\theta_f)$ for comparison.

IV. DISCUSSION

A reasonable starting point for the discussion of the dynamics of a reaction is the basic energetics; how much energy is required for the reaction to occur, or, equivalently, how much energy is released when the products are formed. The disposal of this excess energy is determined by the potential energy surface, and gives some clues to the local shape of the potential. If little or no energy is released in translational energy of the product, the product is either trapped on the surface after it is formed, or translational energy plays little or no role in overcoming the barrier to reaction. Efficient transfer of the excess energy into translation is associated with ''late'' barriers, that is, a transition state relatively far from the surface with the product nearly formed. ''Early'' barriers close to the surface with the reactants relatively far apart are expected to dump more energy into internal states of the molecule.

CO_2 formed by CO oxidation on Rh(111) has considerable excess energy, which, in the simplest one dimensional picture, may be estimated by (see, for example, Fig. 13 in Ref. 2)

$$E_{\text{total}} = -\Delta H_{\text{reaction}} - E_{\text{adsorption}}(\text{CO}) - \frac{1}{2} E_{\text{adsorption}}(\text{O}_2) + E_{\text{activation}}. \quad (7)$$

$\Delta H_{\text{reaction}}$, the total enthalpy of the reaction, is −67.6 kcal/mol. The heat of adsorption of CO on Rh(111) has been measured both by temperature programmed desorption[28] and kinetic measurements;[29] in the limit of low CO coverage, it is 32 kcal/mol. The heat of adsorption of oxygen has also been measured by both these methods,[30,32] in the limit of low coverage it is 56 kcal/mol. The reported value for $E_{\text{activation}}$, the activation energy for CO oxidation, is 24.5 kcal/mol.[6] Using these values, there is expected to be about 32 kcal/mol (1400 meV) of excess energy available for partitioning among the surface and product CO_2 modes. Since the heats of adsorption and the activation energy are expected to change with the coverage of the reactants, the actual value may be quite different. Also, these numbers are averages: if there is more than one mechanism for CO_2 formation on Rh(111), or if the reaction may occur via different paths with different energetics, they may not be characteristic of any particular process or feature on the PES. As will be discussed below, CO oxidation on Rh(111) appears to occur by at least two mechanisms, and the dynamics seem to be better described by a distribution of barrier heights rather than a single one.

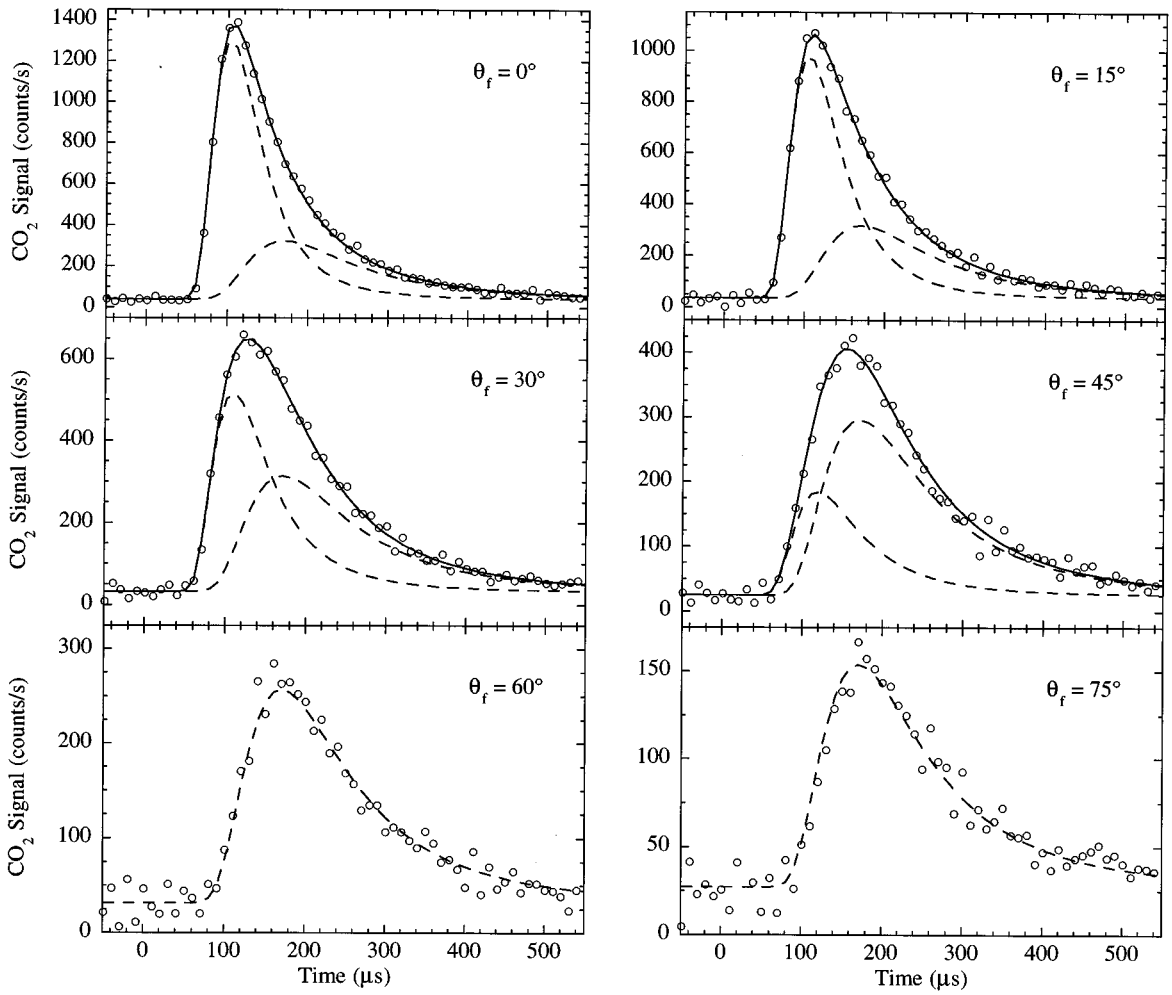

FIG. 5. TOF spectra at T_s=500 K, $\theta_O \sim 0.1$ ML fit to the two peak form in Eq. (6). For $\theta_f \geq 60$, the intensity of the high energy peak is nearly zero, and the TOF spectra are well fit by Maxwell–Boltzmann distributions at 500 K.

A. Origin of the bimodality

Bimodal velocity distributions have been observed for CO oxidation on Pt(111) (Refs. 10–13) and for H_2 recombination on Pd(111)/S.[33] For the latter case, Comsa *et al.* proposed a ''barrier with holes'' model in which molecules which passed through the ''hole'' in the activation barrier emerged with a cosine angular distribution, while those which went over the barrier were focused toward normal and had energies greater than T_s. For the more relevant case of CO oxidation on Pt(111), it was found that the fraction of thermal CO_2 increased with oxygen exposure as the surface oxide of Pt was formed.[10,11] The thermal portion could then be due either to a greater facility of the oxide for trapping the CO_2 as it is formed, or a different mechanism for CO oxidation on the oxidized surface (thus creating a hole in the barrier to CO_2 formation). Rh(111) does not form a surface oxide, and our TOF distributions did not change with oxygen exposure, even though oxygen is absorbed into the bulk. The CO_2 scattering data show that even CO_2 with large amounts of translational energy may be accommodated at surface temperatures from 400 K to 600 K, and the physisorbed CO_2 desorbs with a Maxwellian velocity distribution at T_s. CO_2 formed in the reaction of CO and O on the surface may have even more translational energy, and some energy in internal degrees of freedom as well, but it may be that some geometries allow it to be trapped and its translational energy accommodated before it leaves the surface. The fact that the fraction of thermal CO_2 drops with increasing T_s also seems consistent with a trapping mechanism. Unfortunately, our data provide no way to distinguish between this possibility and a second mechanism for the reaction which has no barrier.

Either way, the fact that some of the CO_2 leaves the surface with no more energy than the surface temperature presents an interesting detailed balance question; it implies that some CO_2 should dissociatively adsorb even at very low translational energies, yet the measured sticking coefficient of CO_2 on Rh(111) is very small. It is possible that the ''thermal'' CO_2 is only accommodated in the translational degree of freedom, and retains excess energy in other modes (which, in the reverse reaction, might make CO_2 stick even at low incident energies) but this question can only be answered by measuring the TOF spectra and internal excitations simultaneously.

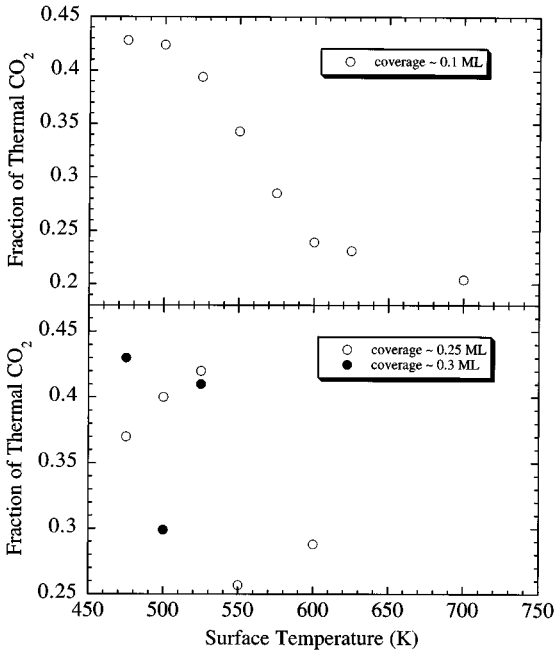

FIG. 6. Fraction of CO_2 (integrated over all desorption angles) desorbing with thermal velocity distributions as a function of surface temperature. The large scatter for the data at higher oxygen coverages is due to lower signal in those measurements.

B. Coverage dependence

The effect of oxygen coverage on the kinetics of CO oxidation on transition metals is pronounced.[1,2] Campbell *et al.* found that the activation energy for CO oxidation on Pt(111) decreases from 24.1 kcal/mol at low oxygen coverages to 11.7 kcal/mol at high oxygen coverages.[3] Similar results have been reported on Rh(110).[34] This change is generally attributed to repulsive interactions between adsorbed oxygen atoms which destabilize the mixed CO–oxygen overlayer, bringing its energy closer to that of the transition state. The observed effects on the dynamics of CO oxidation are generally smaller, except at very high oxygen coverages with different states of chemisorbed oxygen, particularly chemisorbed molecular oxygen.[13] For CO oxidation on polycrystalline Pd, Coulston and Haller measured increases in vibrational and rotational temperatures of ~10%–20% on increasing the oxygen coverage from 0.34 to 0.4 ML.[21] For CO oxidation on Pt, Mantell *et al.*[18,20] found that the vibrational temperature increased with increasing oxygen coverage; Brown and Bernasek[19] observed the opposite effect, and a nonmonotonic dependence of the vibrational temperature on oxygen coverage has also been reported.[22] Our measured velocity distributions likewise show much less dramatic changes than the kinetics. The fraction of CO_2 leaving the surface with thermal velocities decreases, and the average energy of the high energy peak increases by ~10%–15% over an oxygen coverage range of 0.1–0.3 ML. These results are in accord with the idea that the coverage dependence of

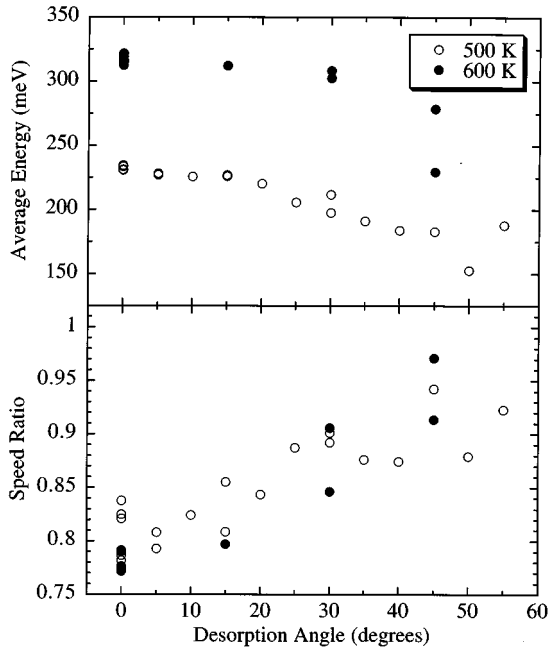

FIG. 7. Angular variation of the average energy and speed ratio of the high energy peak. Open circles, $\theta_O \sim 0.1$ ML, $T_s = 500$ K; filled circles, $\theta_O \sim 0.1$ ML, $T_s = 600$ K.

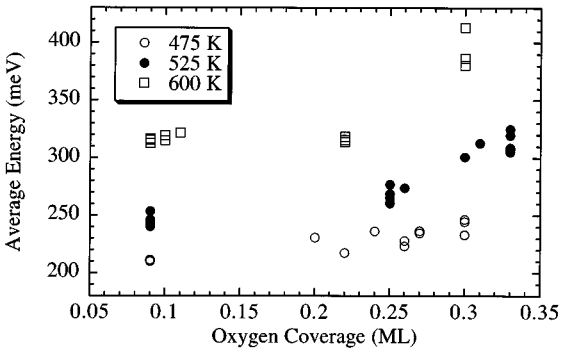

FIG. 8. Average energy of the high energy peak at $\theta_f = 0°$ as a function of oxygen coverage. Open circles, $T_s = 475$ K; filled circles, $T_s = 525$ K; squares, $T_s = 600$ K.

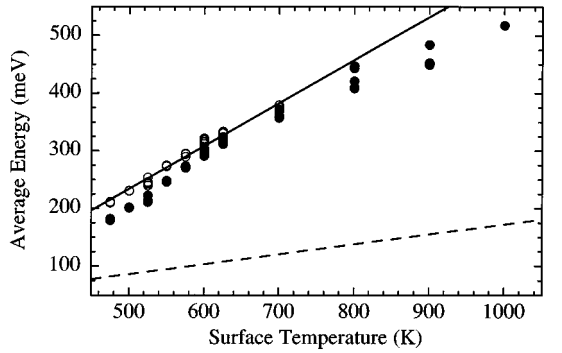

FIG. 9. Average energy of the high energy peak for $\theta_O \sim 0.1$ ML and $\theta_f = 0°$ as a function of surface temperature. Open circles: energy averaged over high energy component. Filled circles: energy averaged over the whole TOF spectrum. Solid line is a linear fit to the data for $T_s \leqslant 700$ K giving $\langle E\ (\text{meV})\rangle = 8.7\ k_b - 139$ meV. The dashed line is the expected energy if the translational temperature is equal to T_s.

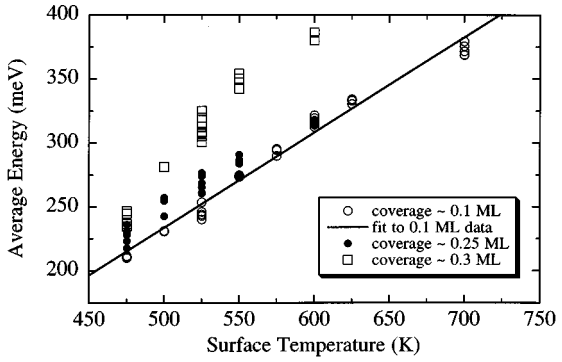

FIG. 10. Average energy of the high energy peak as a function of surface temperature for $\theta_f=0°$ and oxygen coverages as shown.

the kinetics arises largely from a destabilization of the CO–oxygen overlayer; this is equivalent to complementary changes in the heats of adsorption and $E_{\text{activation}}$ in Eq. (7) which should not effect the total excess energy in the product.

C. Angular and temperature dependence of the high-energy peak

That some of the CO_2 should desorb with translational energies well above the surface temperature is not at all unexpected, this behavior has been seen for CO oxidation on polycrystalline Pt (Ref. 9) and Pt(111) (Refs. 10–13) and for hydrogen recombination on Cu,[35–37] Pt,[38] and Pd (Ref. 39) surfaces. This behavior has also been observed for CO oxidation on Rh(111).[7] As mentioned earlier, the most interesting result is the temperature dependence of the velocity distributions, i.e., the fact that the average energy increases so rapidly with surface temperature, and over such a large temperature range.

Measurements of the temperature dependence of time-of-flight distributions are relatively rare because they require a postcrystal chopper to isolate the measurement of the time of flight from the temperature dependent residence time of the reactants. For HD formation on Pt(111), Verheij *et al.*[38] found that the average energy of the desorbing molecules increases with temperature with a slope of $4k_b$. For CO oxidation on Pt(111), Becker[10] reports that the average energy of the product CO_2 increases with T_s with a slope of about $7k_b$, but, since the measurement was made by chopping the CO beam before the crystal, attributes it to the temperature dependence of the CO residence time. Poelmann *et al.*[11,12] have also studied CO oxidation on Pt(111) and report that the average energy of the desorbing CO_2 increases with a slope of $2k_b$, but, again, the measurement was made by chopping the incoming CO beam, and must be corrected for the residence time of the CO. Allers *et al.*[13] have measured velocity distributions of CO_2 formed in steady-state CO oxidation using a postcrystal chopper, but report the average energies for only two surface temperatures; these two points give a slope of $\langle E\rangle$ vs T_s of $5k_b$. The variation in these results for CO oxidation on Pt(111) may be due to difficulties in correcting for the CO residence time in the earlier measurements, or in differences in reactant coverages. The temperature dependence of the average energy that we have observed for CO oxidation on Rh(111) is even steeper, with a slope of $8.7k_b$ for $\theta_O\sim 0.1$ ML and $\theta_f=0°$.

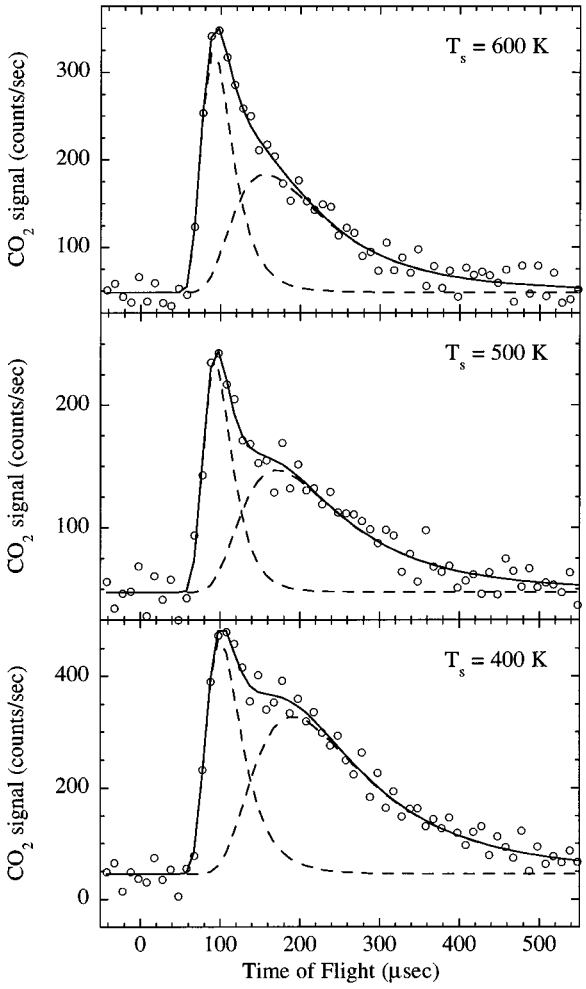

FIG. 11. TOF spectra for CO_2 scattered from the clean Rh(111) surface. For all three spectra, $\theta_i=45°$, $\theta_f=0°$. Fits are to a sum of a shifted Boltzmann for the directly scattered CO_2 and a Maxwell–Boltzmann distribution at T_s for trapped CO_2.

What is expected for the temperature dependence of the energy of desorbing product molecules? Since the velocity distributions are actually a complicated function of the multidimensional potential surface, it is difficult to create an adequate analytic model. The simplest model, due to van Willigen,[40] assumes a one-dimensional barrier in the direction normal to the surface; only molecules with sufficient normal energy to overcome the barrier desorb. The predicted velocity distributions are just the high energy tail of a Maxwell–Boltzmann at the surface temperature. For a barrier height, E_b, much greater than $2k_bT_s$, this model predicts the average energy of molecules desorbing at normal will be

$$\langle E\rangle = E_b + 2k_bT_s, \tag{8}$$

which is much weaker than that observed for the current system.

Another one-dimensional model proposed by Doyen[41] with important refinements by Verheij *et al.*[38] and Anger *et al.*,[42] relates the energy of the desorbing molecules to the angular distribution using a simple model for the interaction of the desorbing molecules with the surface phonons. For a $\cos^9(\theta_f)$ angular distribution, this model predicts that the slope of $\langle E \rangle$ vs T_s will be $6k_b$, which is still not as steep as the observed T_s dependence.

D. Surprisal analysis

In one sense, the failure of these very simple models to reproduce the data are expected. They are based on one-dimensional barriers and consider only translational energy. CO_2 may not be well represented by a structureless particle; it is probably formed in a bent configuration on the surface, with considerable energy released in internal modes as well as translation. In the absence of a simple model, the first question to be answered is how much information can actually be extracted from the velocity and angular distributions. Are the observed velocity distributions at different temperatures and angles the result of complicated interactions between internal and translational modes of the molecules and surface phonons, or is there a model involving only a few aspects of the PES which will account for the data? On a more practical level, how many independent parameters can we derive from the measured distributions?

Surprisal analysis is a standard tool for answering these questions which has been extensively used in studies of gas phase dynamics, and it has also been used to analyze vibrational energy distributions in CO and CO_2 from oxidation of C and CO on Pt.[43,44] There are excellent explanations in textbooks[45] and review articles on the subject[46,47] and the specifics of applying surprisal analysis to angular[48] and velocity[49] distributions have been discussed previously so only the primary result will be presented here.

The functional form for the ''most random'' possible distribution subject to some (small) number of constraints is

$$f_m(i) = f_0(i) \exp\left[-\sum_n \lambda_n A_n(i) \right], \tag{9}$$

where $f_m(i)$ is the measured distribution, the λ_n are the surprisal parameters, the A_n are the constrained variables, and $f_0(i)$ is the ''prior'' distribution, the most random possible distribution in the absence of any constraint. Another useful quantity is the information content of the distribution, or ''surprisal'' which is defined as

$$I(i) = -\ln\left[\frac{f_m(i)}{f_0(i)} \right] = \lambda_1 A_1 + \lambda_2 A_2 + \cdots . \tag{10}$$

If a particular measured distribution can be defined by a single parameter, a plot of its surprisal vs i will be linear.

To apply surprisal analysis, one must choose a prior distribution and make an educated guess about the constraints. For the case of molecules desorbing from a surface, a logical choice for the prior distribution is that which arises from ''equilibrium'' desorption, where the desorbing molecules have accommodated at the surface temperature,

$$f(v) = N v^3 \cos(\theta_f) \exp\left(\frac{-m v^2}{2 k_b T_s} \right). \tag{11}$$

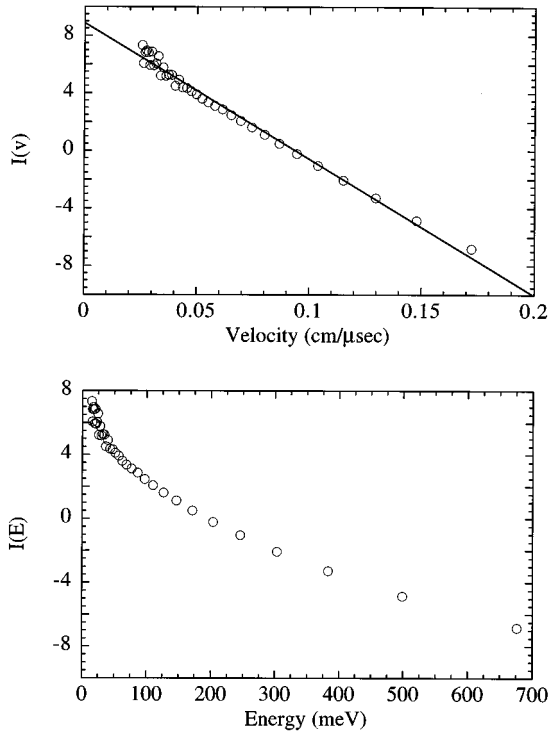

FIG. 12. Surprisal plot of the velocity distribution measured with $T_s = 500$ K, $\theta_O \sim 0.1$ ML, and $\theta_f = 0°$. The Maxwell–Boltzmann distributed part of the distribution has been subtracted, and the intensities are flux corrected, but the ionizer broadening has not been deconvoluted out. The solid line is a linear fit to the data.

Given that the angular distributions of product CO_2 are peaked along the surface normal, and that the translational energies are greater than the surface temperature, there must be some constraint on θ_f and also on the velocity or energy. Determining the form of the constraint is a matter of trial and error, looking for the particular form which gives the surprisal plot which may be fit with the fewest parameters. Surprisal plots for the TOF spectrum at $T_s = 500$ K, $\theta_f = 0°$, and $\theta_O \sim 0.1$ ML (with the thermal fraction subtracted) are shown in Fig. 12. In the top panel, the constrained parameter is the velocity and in the bottom panel it is the energy; clearly, a constraint on the velocity gives a linear surprisal. Surprisal plots of the angular distribution of the intensity of the high energy peak at $T_s = 500$ K and $\theta_O \sim 0.1$ ML are shown in Fig. 13. In the top panel the constrained parameter is $\cos(\theta_f)$ and in the bottom panel it is $\cos^2(\theta_f)$, corresponding to constraints on the normal velocity and the normal energy. Both of the surprisal plots of the angular distribution are close to linear; on trying to fit the distributions, however, we found that only $\cos(\theta_f)$ came close to reproducing the data. Constraints on $\cos(\theta_f)$ and the velocity suggest $v \cos(\theta_f)$, the normal velocity, as the constraint defining the velocity and

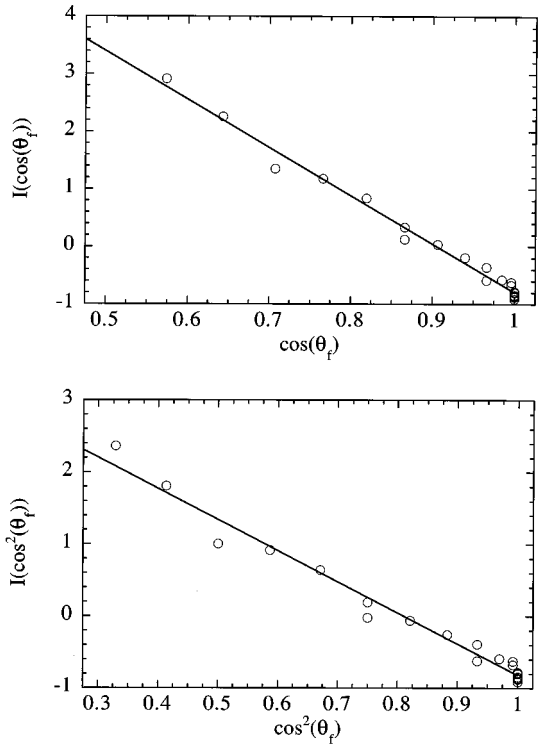

FIG. 13. Surprisal plots of the angular distribution of the intensity of the high energy CO_2 peak for $T_s=500$ K and $\theta_O\sim 0.1$ ML. Solid lines are linear fits to the data.

angular distributions. The functional form this result implies is, using Eq. (9) and dropping the negative in the exponent so λ is positive,

$$f(v,\theta_f)=N_1 f_0(v,\theta_f)\exp[\lambda v\ \cos(\theta_f)]+N_2 f_0(v,\theta_f), \tag{12}$$

where the second term is included to account for the thermally distributed CO_2. This form fits our TOF distributions very well; examples at $T_s=500$ K and $T_s=600$ K are shown in Figs. 14 and 15. Note that only three parameters are needed to fit all of the TOF distributions at a given temperature and coverage; N_1, N_2, and λ do not depend on desorption angle. In contrast, the parameters of the shifted Boltzmanns with which we fit these distributions before were angle dependent—we needed 16 parameters to fit the data in Fig. 14.

The aspect of the dynamics that we are most interested in illuminating, however, is the temperature dependence. λ is plotted as a function of temperature in Fig. 16. There is some scatter in the data, some of which is due to the difficulty in reproducing the same oxygen coverage at different T_s, but there is no clear trend with T_s. One way to gauge the importance of the scatter is to look at the average energies predicted by a constant value of λ as a function of temperature. This is shown, along with the $\theta_O\sim 0.1$ ML data, in Fig. 17; the value of λ is 68.3 μs/cm, just a simple average over all of the $\theta_O\sim 0.1$ ML points in Fig. 16. Although the data are not reproduced exactly with a constant value of λ, the slope of $\langle E\rangle$ vs T_s is $8.5k_b$, very close to the experimental value. Essentially, all of the dynamics of the "fast" CO_2 at $\theta_O\sim 0.1$ ML, for $T_s=475$ K–700 K and the entire angular range, can be condensed into a single parameter. Although the actual potential energy surface is at least nine dimensional (and has many more dimensions when the surface degrees of freedom are considered) either the thermal averaging or the dominance of a single feature of the PES results in velocity distributions which are sensitive only to a single parameter, a constraint on the value of the velocity in the direction normal to the surface, $v\cos(\theta_f)$.

For surface temperatures greater than 700 K, the CO_2 signal is too small to measure the TOF spectra at large desorption angles, and thus it is difficult to determine the relative intensities of the thermal and high energy components. Without this information, it is not possible to obtain a unique fit to Eq. (12) to determine the value of λ. However, the fact that the average energy is decreasing more slowly with surface temperature indicates that, if the velocity distributions may still be fit to Eq. (12), λ must decrease. This may indicate that at such high temperatures, we are approaching the limit where everything on the surface has a high probability of reacting.

The surprisal form in Eq. (12) also fits the data at higher oxygen coverage, at least for the range where we have sufficient data to determine the relative intensities of the high energy and thermal components. The values for the surprisal parameter for $\theta_O\sim 0.25$ ML, and $\theta_O\sim 0.3$ ML are also plotted in Fig. 16. The scatter in the values of the surprisal parameter is more severe than for the $\theta_O\sim 0.1$ ML data, due in part to lower signal and greater difficulties in reproducing the same coverages at different surface temperatures. In general, it appears that λ increases with increasing oxygen coverage.

E. Interpretation of the constraint

One drawback of surprisal analysis is that, by itself, it does not provide a physical model for the dynamics. All of the physical insight that it yields is in the constraints that must be applied to fit the distributions. However, it also yields the important fact that only one independent parameter can be determined from the data. Therefore, while the data may be fit with a model containing many adjustable parameters, the fit will not be unique, and more than one parameter cannot be determined unambiguously.

The most straightforward interpretation of the data comes from the application of detailed balance, which states that, for a system at equilibrium, the desorbing flux must be identical to the adsorbing flux,[50] so that the sticking coefficient as a function of velocity and desorption angle is given by

$$s(v,\theta_f)=\frac{\text{velocity distribution of desorbing molecules}}{\text{velocity distribution of a gas at } T_s \text{ incident on the surface}}\propto \exp[\lambda v\ \cos(\theta_f)]+\text{constant}. \tag{13}$$

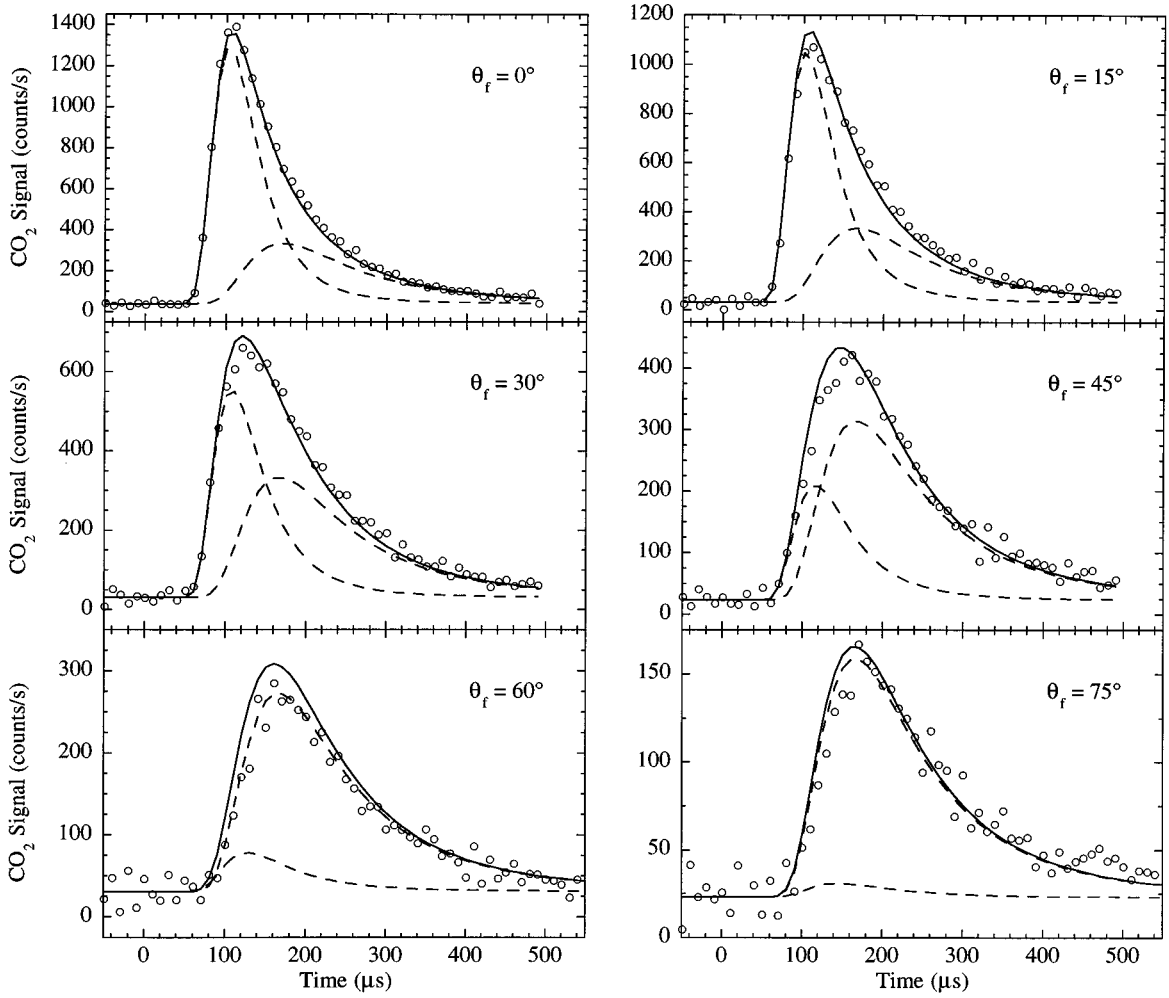

FIG. 14. TOF spectra at T_s=500 K, $\theta_O \sim 0.1$ ML; fits are to the surprisal form in Eq. (12).

The constant term corresponds to the thermal fraction of the desorbing CO_2, and the probability of an incident CO_2 dissociating to form adsorbed carbon monoxide and oxygen increases exponentially with increasing normal velocity. Clearly, this dependence cannot hold at all velocities, since the sticking coefficient must be less than or equal to one, but it holds in the energy range observed for the desorbing CO_2, ~200–350 meV. This is a very steep dependence of the sticking coefficient on the energy; for H_2/Pt(111), for example, $S[E\cos^2(\theta_f)] \propto [E\cos^2(\theta_f)]^2$.[38]

The energy dependence of the sticking coefficient is frequently interpreted in terms of a distribution of barrier heights in a one-dimensional potential.[51,52] If there is only a single path through the PES which leads to dissociative adsorption, then there is a single barrier, and the sticking coefficient will be a step function in the energy. If there are multiple reaction paths, each will have its own barrier height, and, generally, one expects there to be more possible paths to reaction at higher energies. Formally, this distribution of barrier heights is defined by the equation [see Ref. 51 and Eq. (4) of Ref. 52]

$$S(E) = \int_0^E \sigma(E')dE'. \tag{14}$$

Restating this in differential form and plugging in the energy dependence of the sticking coefficient from Eq. (13) yields

$$\sigma(E) = \frac{dS}{dE} \propto \frac{\lambda}{2\sqrt{E}} \exp(\lambda\sqrt{E}) \tag{15}$$

for this system. Extracting any information about the potential surface that creates this distribution of barrier heights requires more assumptions. If the PES can be represented by a two dimensional surface, the transition state is a saddle point, and $\sigma(E)$ is related to the width of the channel at the transition state. More precisely, it should be the arc length of the cross section of the saddle perpendicular to the reaction path. From the standard formula for the arc length,

$$\sigma(E)dE = dS = \sqrt{(dx)^2 + (dE)^2}$$

or

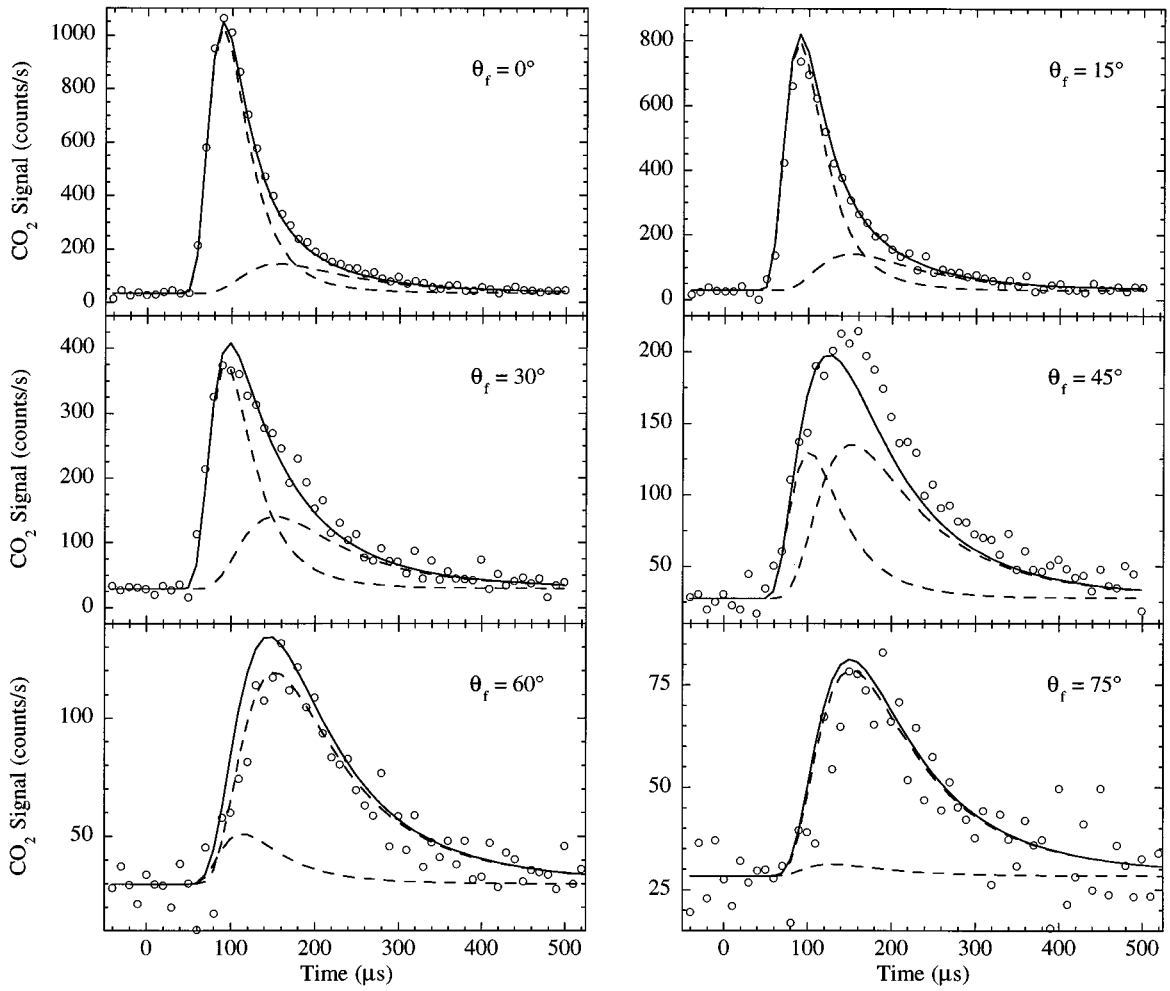

FIG. 15. TOF spectra at T_s=600 K, $\theta_O \sim 0.1$ ML; fits are to the surprisal form in Eq. (12).

$$\frac{dS}{dE} = \sqrt{1+\left(\frac{dx}{dE}\right)^2}, \tag{16}$$

where x is some variable, or combination of variables, in the geometry of the reaction; it could be the length of a carbon–oxygen bond, or the bond angle, or some other parameter.

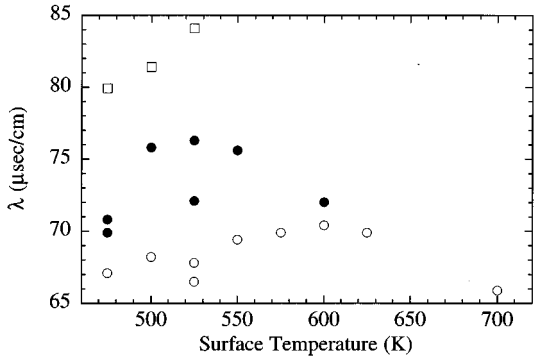

FIG. 16. Temperature dependence of the surprisal parameter, λ. Filled circles, $\theta_O \sim 0.1$ ML; open circles, $\theta_O \sim 0.25$ ML; squares, $\theta_O \sim 0.3$ ML.

Equations (16) and (17) relate the energy dependence of the sticking coefficient to the local shape of the PES. Explicitly, this may be stated

$$\frac{dx}{dE} = \sqrt{\left(\frac{dS}{dE}\right)^2 - 1}. \tag{17}$$

This formula may be integrated to give the shape of the saddle point which is consistent with a given $S(E)$. It is only valid for limited energy ranges; for large energies where $S(E)$ levels off, it clearly cannot hold. However, its predictions for the local geometry are reasonable. If $S(E)$ looks like a step function, $E(x)$ increases steeply; the PES near the transition state is a narrow channel with steep sides, approaching the one dimensional limit where is there is only a single possible reaction path. If $S(E)$ increases over a large energy range, the calculated $E(x)$ varies more slowly, so that increasing the energy opens up many new paths for the reaction.

Dissociative sticking of CO_2 (and hence CO oxidation) fall into the latter category. $E(x)$ for the average values of λ obtained for $\theta_O \sim 0.1$ ML, $\theta_O \sim 0.25$ ML, and $\theta_O \sim 0.3$ ML are shown in Fig. 18. The same values for the pre-exponential

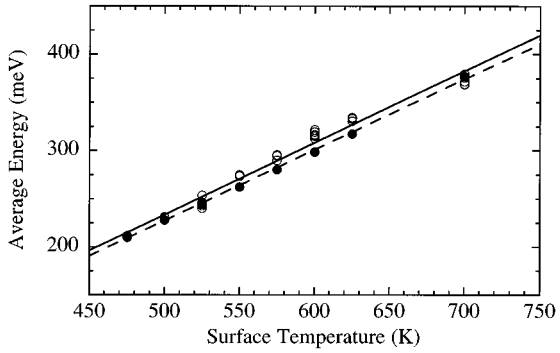

FIG. 17. Comparison of measured average energies for $\theta_O \sim 0.1$ ML, $\theta_f = 0°$ (open circles) with those calculated with $\lambda = 68.3$, independent of T_s (filled circles). Solid line is a linear fit to the data, as in Fig. 9. Dashed line is a linear fit to the calculated values which gives $\langle E \rangle$ (meV)$= 8.5\ k_b T_s - 139.9$ meV.

and the barrier height (the lowest possible energy at which the reaction may occur) are assumed at all three coverages. As expected, the potentials for the higher coverages vary more slowly, so that higher energy CO_2 has a much higher sticking probability. Figure 18 is interesting primarily in that it suggests a second possible interpretation of the coverage dependence of the dynamics. Instead of destabilizing the transition state, as suggested in the last section, the higher oxygen coverage could give rise to higher energy CO_2 by changing the shape of the potential.

Attempting to interpret the distribution of barrier heights in this way is clearly open to question. The most important objection is that the PES may not be well represented by a two dimensional surface; if more dimensions must be taken into account, $\sigma(E)$ is related to a volume in the potential space, and the problem becomes much more complicated. Another difficulty is that the information yielded is very limited. Nothing whatever may be inferred about the shape of the barrier along the reaction coordinate. The all important geometric variable which is perpendicular to the reaction coordinate is also unknown. The reaction probability is a function of the normal velocity and a great deal of energy winds up in translation which both suggest a barrier relatively far from the surface (i.e., an early barrier for dissociative sticking and a late barrier for CO_2 formation). Thus the reaction coordinate might be expected to roughly parallel to the surface normal. The geometry of the transition state is unknown, but is probably bent and bound to the surface either through a single oxygen or the carbon and an oxygen atom.[53,54] It may also carry a partial negative charge—the CO_2^- ion is known to dissociate readily into CO and O on K doped Rh surfaces[55] and is a reasonable guess for an intermediate. In short, there are plenty of possible candidates for a second crucial geometric parameter, and the current data provide no way to pick one.

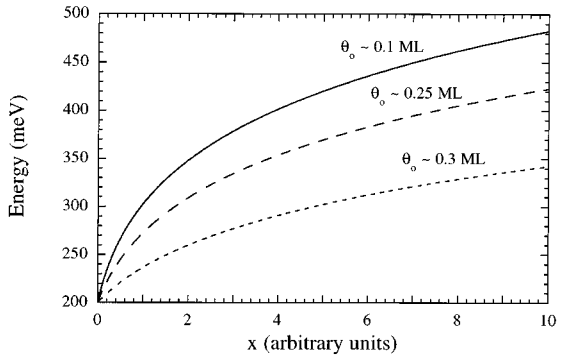

FIG. 18. Comparison of integrated potentials from Eq. (17) for $\theta_O \sim 0.1$ ML (solid line), $\theta_O \sim 0.25$ ML (dashed line), and $\theta_O \sim 0.3$ ML (short-dashed line). The constant of integration, which corresponds to the lowest possible barrier in the translational degree of freedom, has been arbitrarily set to 200 meV for all three coverages. $x = 0$ represents the "equilibrium" position of x, the value of x for which the energy is lowest. For negative x, the potential is expected to increase steeply.

Another possibility suggested by the exponential dependence of $S(E)$ is that tunneling may play some role in sticking and dissociation. A model based on tunneling through a parabolic barrier will not fit the data, because it yields an exponential dependence of the sticking coefficient on v^2, which is too steep, but tunneling through a square barrier gives about the right slope of S vs $v\cos(\theta_f)$ and actually does fit the data fairly well at low energies. A square barrier model, of course, involves two parameters, the height of the barrier and the width. In order to determine both, it is necessary to incorporate more information—ideally the absolute value of the dissociative sticking probability of CO_2. We looked for dissociative sticking of CO_2 and did not observe any, even at incident energies of 430 meV. The sticking probability has been measured at high pressures of CO_2 and H_2 (1 Torr CO_2, 100 Torr H_2) by Goodman *et al.*;[56] for $T_s = 470$ K under these conditions, the sticking coefficient is $\sim 10^{-8}$. Parameters for a square barrier can be found which give this value for the sticking coefficient and fit our TOF data; they are 810 meV for the barrier height and 0.058 Å for the barrier width. Such a narrow barrier width is difficult to justify physically; in comparison, the width of a parabolic barrier needed to fit methane dissociation on Ni(111) is ~ 0.4 Å.[57] Such a tall thin barrier corresponds to an extremely steep, not very realistic potential, so this simple model suggests tunneling is not playing a very large role.

V. CONCLUSIONS

We have measured the velocity distributions of CO_2 as a function of desorption angle, surface temperature, and oxygen coverage. Using a postcrystal chopper and continuous beams of CO and oxygen allow these measurements to be made under steady-state conditions; constant CO and oxygen coverages and constant surface temperature. We have found that both the angular and velocity distributions appear to be bimodal. One component is well characterized by Maxwell–Boltzmann velocity distributions at the surface temperature and a cosine angular distribution. The second component is non-Boltzmann, with energies much greater than expected for molecules which have equilibrated with the surface, and an angular distribution sharply peaked toward normal. The average energy of the high energy peak increases slowly with oxygen coverage. The average energy of the high energy peak is a very strong function of surface temperature. At an

oxygen coverage of 0.1 ML and desorption angle of 0°, it increases with a slope of $8.7k_b$ between 450 and 700 K, more than four times the slope expected for molecules accommodated on the surface. At higher oxygen coverages, the slope is even larger.

Surprisal analysis of the high energy component shows that, for temperatures below 700 K and $\theta_O \sim 0.1$ ML, the velocity and angular distributions may be characterized by a single constraint on the normal velocity, $v\cos(\theta_f)$. Although the system is a very complex one, the dynamics of the high energy peak at this coverage and in this temperature range may be described by a single parameter; the predictions coming from this model provide a global, quantitative description of the data. The results are similar at higher coverages, but with different values of the surprisal parameter. A knowledge of the internal states is necessary for a complete interpretation, but direct application of detailed balance to this result suggests that the sticking coefficient of CO_2 on Rh(111) increases exponentially with normal velocity. This energy dependence of the sticking coefficient may be interpreted as a rapid increase in the distribution of barrier heights with energy, corresponding to a wide, shallow channel in the potential energy surface near the transition state.

ACKNOWLEDGMENTS

J.I.C. acknowledges financial support from AT&T Bell Laboratories through the Graduate Research Program for Women. Acknowledgment is made to the donors of The Petroleum Research Fund, administered by the ACS, for partial support of this research. This work was also supported in part by the Materials Research Science and Engineering Center Program of the National Science Foundation under award DMR-9400379.

[1] T. Engel and G. Ertl, Adv. Catal. **28**, 1 (1979).
[2] T. Engel and G. Ertl, in *The Chemical Physics of Solid Surfaces and Heterogeneous Catalysis*, edited by D. A. King and D. P. Woodruff (Elsevier, New York, 1982).
[3] R. L. Palmer and J. N. Smith, Jr., J. Chem. Phys. **60**, 1453 (1974).
[4] C. T. Campbell, G. Ertl, H. Kuipers, and J. Segner, J. Chem. Phys. **73**, 5862 (1980).
[5] J. Segner, C. T. Campbell, G. Doyen, and G. Ertl, Surf. Sci. **138**, 505 (1984).
[6] L. S. Brown and S. J. Sibener, J. Chem. Phys. **89**, 1163 (1988).
[7] L. S. Brown and S. J. Sibener, J. Chem. Phys. **90**, 2807 (1989).
[8] T. Engel and G. Ertl, J. Chem. Phys. **69**, 1267 (1978).
[9] C. A. Becker, J. P. Cowin, L. Wharton, and D. J. Auerbach, J. Chem. Phys. **67**, 3394 (1977).
[10] C. A. Becker, Ph.D. thesis, 1980.
[11] E. Poelmann, Ph.D. thesis, 1992.
[12] E. Poelmann, M. Schmitt, and H. Hoinkes, Surf. Sci. **287/288**, 269 (1993).
[13] K.-H. Allers, H. Pfnür, P. Feulner, and D. Menzel, J. Chem. Phys. **100**, 3985 (1994).
[14] T. Matsushima, K. Shobatake, and Y. Ohno, Surf. Sci. **283**, 101 (1993).
[15] Y. Ohno, T. Matsushima, and H. Uetsuka, J. Chem. Phys. **101**, 5319 (1994).
[16] D. A. Mantell, S. B. Ryali, B. L. Halpern, G. L. Haller, and J. B. Fenn, Chem. Phys. Lett. **81**, 185 (1981).
[17] S. L. Bernasek and S. R. Leone, Chem. Phys. Lett. **84**, 401 (1981).
[18] D. A. Mantell, S. B. Ryali, and G. L. Haller, Chem. Phys. Lett. **102**, 37 (1983).
[19] L. S. Brown and S. L. Bernasek, J. Chem. Phys. **82**, 2110 (1985).
[20] D. A. Mantell, K. Kunimori, S. B. Ryali, G. L. Haller, and J. B. Fenn, Surf. Sci. **172**, 281 (1986).
[21] G. W. Coulston and G. L. Haller, J. Chem. Phys. **95**, 6932 (1991).
[22] G. K. Kunimori and G. L. Haller, Bull. Chem. Soc. Jpn. **65**, 2450 (1992).
[23] K. D. Gibson and S. J. Sibener, J. Chem. Phys. **88**, 7862 (1988).
[24] D. F. Padowitz and S. J. Sibener, Surf. Sci. **254**, 125 (1991).
[25] D. D. Koleske and S. J. Sibener, Rev. Sci. Instrum. **63**, 1 (1992).
[26] W. H. Press, B. P. Flannery, S. A. Teukolsky, and W. T. Vetterling, *Numerical Recipes* (Cambridge University, Cambridge, 1989).
[27] C. T. Reimann, M. El-Maazawi, K. Walzel, B. J. Garrison, N. Winograd, and D. M. Deaven, J. Chem. Phys. **90**, 2027 (1989).
[28] P. A. Thiel, E. D. Williams, J. T. Yates, and W. H. Weinberg, Surf. Sci. **84**, 54 (1979).
[29] K. A. Peterlinz, T. J. Curtiss, and S. J. Sibener, J. Chem. Phys. **95**, 6972 (1991).
[30] P. A. Thiel, J. T. Yates, and W. H. Weinberg, Surf. Sci. **82**, 22 (1979).
[31] J. T. Yates, P. A. Thiel, and W. H. Weinberg, Surf. Sci. **82**, 45 (1979).
[32] K. A. Peterlinz, Ph.D. thesis, 1993.
[33] G. Comsa and R. David, Chem. Phys. Lett. **49**, 512 (1977).
[34] M. Bowker, Q. Guo, and R. W. Joyner, Surf. Sci. **280**, 50 (1993).
[35] G. Comsa and R. David, Surf. Sci. **117**, 77 (1982).
[36] D. J. Auerbach, C. T. Rettner, and H. A. Michelson, Surf. Sci. **283**, 1 (1993).
[37] H. A. Michelson, C. T. Rettner, D. J. Auerbach, and R. N. Zare, J. Chem. Phys. **98**, 8294 (1993).
[38] L. K. Verheij, M. B. Hugenschmidt, A. B. Anton, B. Poelsema, and G. Comsa, Surf. Sci. **210**, 1 (1989).
[39] L. Schröter, C. Trame, R. David, and H. Zacharias, Surf. Sci. **272**, 229 (1992).
[40] W. van Willigen, Phys. Lett. A **28**, 80 (1968).
[41] G. Doyen, Vacuum **32**, 91 (1982).
[42] G. Anger, A. Winkler, and K. D. Rendulic, Surf. Sci. **220**, 1 (1989).
[43] M. Kori and B. Halpern, Chem. Phys. Lett. **129**, 407 (1986).
[44] B. Halpern and M. Kori, Chem. Phys. Lett. **138**, 261 (1987).
[45] J. I. Steinfeld, J. S. Francisco, and W. L. Hase, *Chemical Kinetics and Dynamics*, (Prentice–Hall, Englewood Cliffs, 1989).
[46] R. D. Levine, Annu. Rev. Phys. Chem. **29**, 59 (1978).
[47] R. D. Levine and J. L. Kinsey, in *Atom–Molecule Collision Theory: A Guide for the Experimentalist*, edited by R. B. Bernstein (Plenum, New York, 1978).
[48] M. B. Faist, R. D. Levine, and R. B. Bernstein, J. Chem. Phys. **66**, 511 (1977).
[49] E. Pollak and R. D. Levine, Chem. Phys. **21**, 61 (1977).
[50] G. Comsa and R. David, Surf. Sci. Rep. **5**, 145 (1985).
[51] M. Balooch, M. J. Cardillo, D. R. Miller, and R. E. Stickney, Surf. Sci. **46**, 358 (1974).
[52] K. D. Rendulic, G. Anger, and A. Winkler, Surf. Sci. **208**, 404 (1989).
[53] N. K. Ray and A. B. Anderson, Surf. Sci. **119**, 35 (1982).
[54] D. W. J. Kwong, N. DeLeon, and G. L. Haller, Chem. Phys. Lett. **144**, 533 (1988).
[55] F. Solymosi and G. Klivény, Catal. Lett. **22**, 337 (1993).
[56] D. W. Goodman, D. E. Peebles, and J. M. White, Surf. Sci. **140**, L239 (1984).
[57] M. B. Lee, Q. Y. Yang, and S. T. Ceyer, J. Chem. Phys. **87**, 2724 (1987).